Iron loss simulation using a local material model

Benedikt Groschup, Silas Elfgen and Kay Hameyer
Institute of Electrical Machines,
Rheinisch Westfalische Technische Hochschule Aachen, Aachen, Germany

Received 17 October 2018
Revised 8 January 2019
Accepted 14 January 2019

Abstract

Purpose – The cutting process of the electric machine laminations causes residual mechanical stress in the soft magnetic material. A local magnetic deterioration can be observed and the resulting local and global iron losses increase. A continuous local material model for the consideration of the changing magnetization properties has been introduced in a previous work as well as an *a priori* assessment of iron losses. A local iron loss calculation considering both a local magnetization and local loss parameters misses yet. The purpose of this study is to introduce a local iron loss calculation model considering both a local magnetization and local loss parameters.

Design/methodology/approach – In this paper, an approach for local iron loss simulation is developed and a comparison to the cut-edge length-dependent loss model is given. The comparison includes local loss distribution in the lamination as well as the impact on the overall motor efficiency and vehicle range in an electric vehicle driving cycle.

Findings – For an analysis of the resulting local iron loss components, both the local magnetization and iron loss parameters must be considered using physically based models. Consistently, a local iron loss model is presented in the work. The developed model can be used to gain detailed information of the local loss distribution inside the machine. The comparability of this local iron loss with the cut-edge length approach for overall system characteristics, e.g. efficiency or driving range, is shown.

Originality/value – A local iron loss simulation approach is a physical accurate model to describe the influence of cutting techniques on electric machine characteristics. A comparison with the less complicated *a priori* assessment gives detailed information about the necessity of the local model under consideration of the given problem.

Keywords Local iron loss model, Continuous material model, Cut edge (CE), Cutting, Iron losses, Permanent magnet synchronous machine (PMSM), Soft magnetic material

Paper type Research paper

1. Introduction

In standard electric machine simulations and standard iron loss models (STM) such as the Insitut of Electrical Machines (IEM)-formula (Steentjes *et al.*, 2013), the influences of cutting techniques on electromagnetic properties are not considered. However, the IEM-formula can be extended to take the cutting effect into account. Material degradation resulting from cutting processes such as shear or laser cutting introduces magnetic deterioration because of residual stress (Maurel *et al.*, 2003; Siebert *et al.*, 2013). As soft magnetic materials are prone to mechanical stress, both the magnetic permeability and the resulting iron losses are affected (Bali and Muetze, 2017; Siebert *et al.*, 2014; Schoppa *et al.*, 2000). In the state-of-the-art magnetic simulation of electric machines, a local consideration of material properties can be used to solve the field equation (Elfgen *et al.*, 2016b). In the state of the art of loss calculation, global loss parameters are determined to account for the local magnetic deterioration of the material and hence the increase of local iron losses (Elfgen *et al.*, 2017). As the selection of global loss parameters is based on the cut-edge length of the application, this model is referenced as cut-edge length-dependent loss model (CLM) in the following

COMPEL - The international journal for computation and mathematics in electrical and electronic engineering
Vol. 38 No. 4, 2019
pp. 1224-1234

0332-1649
DOI 10.1108/COMPEL-10-2018-0421

study. Local effects such as different width of stator teeth or local phenomena in the rotor are not considered. Therefore, calculation errors are unavoidable. This contribution presents an approach to consider both the local magnetization and local loss parameters. The newly developed local iron loss model (LIM) is introduced and compared with the state-of-the-art STM and CLM.

2. Magnetic measurements

The magnetic properties of the iron material are measured using a single sheet tester (SST) (DIN German Institute for Standardization, 2010). To consider the material degradation arising from the cutting process, SST specimens of equal sizes are cut into different amounts of strip width b. Elfgen *et al.* (2016a, 2016b) depicts the sample preparation. The cross section is kept constant, and specimens are cut parallel and perpendicular to the rolling direction (Figure 1).

Magnetic measurements are carried out according to standards from quasi-static excitation up to 1 kHz. The STM presented in Steentjes *et al.* (2013) are used and parameterized by the measured data. The total iron loss P_{Fe} is calculated using the IEM-formula introduced in Eggers *et al.* (2012). In addition to the classical iron loss calculation from Bertotti (1988), considering the static hysteresis P_{hyst}, eddy current P_{cl} and an excess P_{exc}, the loss term (1)–(4) and the saturation loss term P_{sat} (5) are introduced. They account for the discrepancies arising between measured and estimated iron losses at frequencies above 400 Hz at high polarization values:

$$P_{\mathrm{Fe}} = P_{\mathrm{hyst}} + P_{\mathrm{cl}} + P_{\mathrm{exc}} + P_{\mathrm{sat}} \tag{1}$$

$$P_{\mathrm{hyst}} = \sum_{i=1}^{N} a_1(\xi)\left(1 + \frac{B_{\min}(x_i)}{B_{\max}(x_i)}\left(r_{\mathrm{hyst}} - 1\right)\right) B_{\max}^{\alpha(\xi)}(x_i) f_1 \tag{2}$$

$$P_{\mathrm{cl}} = a_2 \sum_{\mathrm{i}=1}^{N} \sum_{n=1}^{\infty} \left(B_{\mathrm{n}}^2 (nf)^2\right) \tag{3}$$

$$P_{\mathrm{exc}} = \sum_{\mathrm{i}=1}^{N} a_5(\xi) \sum_{n=1}^{\infty} \left(B_{\mathrm{n}}^{1.5} (nf)^{1.5}\right) \tag{4}$$

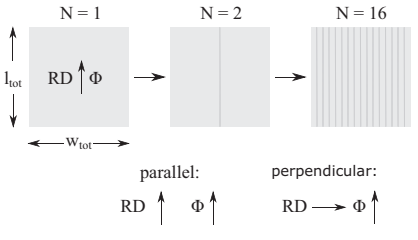

Figure 1.
Single sheet samples of M270-35A with different cutting length

$$P_{\mathrm{sat}} = a_2 \sum_{\mathrm{i}=1}^{N} a_3(\xi) B_{\max}^{a_4(\xi)+2}(x_i) f_1^2 \tag{5}$$

with $\xi = S, x$ being two different variables for the two different models used in this paper, namely, cut-edge length, S being used for the global approach and x being used for the local model. The parameter a_i with $i = 1, . ,5$ and α are the iron loss parameters and address the different loss mechanisms. They correspond to the parameters in (12). In addition, the rotating local flux density is considered with r_{hyst} as presented in Steentjes *et al.* (2012). In SST measurement sheets with a total width and a length $l_{tot} = w_{tot}$ of 120 mm are used. In this study, electrical sheets of the material M270-35A are cut in strip width w_{st} from 4 to 120 mm in a total of six steps using guillotine shears. The cutting and measuring process is performed as introduced in Elfgen *et al.* (2017). Both B_{max}–H_{max} curves and losses are determined for each strip width. The cutting length S_{SST} is calculated as:

$$S_{\mathrm{SST}} = 2\, w_{\mathrm{tot}} + 2 \frac{w_{\mathrm{tot}}}{w_{\mathrm{st}}} l_{\mathrm{lot}} \tag{6}$$

The specific losses P_s of the sheet in dependency of the cutting-edge length of the SST probe S_{SST} and the polarization J are shown in Figure 2. The specific losses P_s show a linear dependency of the total cutting-edge length S.

3. Finite element modelling simulation model

3.1 Local material model

In Elfgen *et al.* (2016a), the authors present a continuous local material model (LMM) considering the cut-edge effect in terms of a local permeability. This model is used to consider the manufacturing influence in terms of a local permeability within the application. As a consequence of a mechanical or thermal cut, the magnetic flux density B (x, H, f) written in (7) becomes dependent on the location x, the undamaged permeability $\mu_{\mathrm{r,u}}$, the permeability drop at the cut edge $\Delta\mu_{\mathrm{cut}}$ and the deterioration profile η (x):

$$B(x, H, f) = \mu_0 H\left(\mu_{\mathrm{r,u}}(H, f) - \Delta\mu_{\mathrm{cut}}(H, f)\, \eta(x)\right) \tag{7}$$

The influence of the local stress on the permeability in terms of the necessary magnetization field strength H is reflected in a decreasing permeability. The permeability drop at the cut edge in (8) is a function of the material and processing parameters, as it does not depend on the strip width of the specimen:

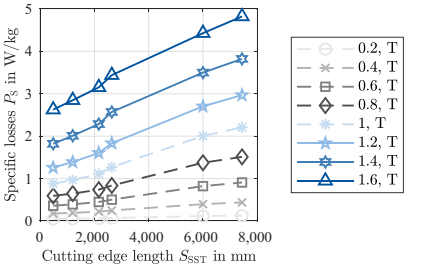

Figure 2.
Specific losses of M270-35A measured in parallel to the rolling direction

$$\Delta\mu_{\mathrm{cut}}(H,f) = \frac{\mu_{\mathrm{r,u}}(H,f) - \mu_{\mathrm{r}}(b,H,f)}{F(b,f)} \tag{8}$$

By identifying $F(b)$, the discrepancy of the quotient for each characterized specimen is minimized. $F(b,f)$ F(b,f) as shown in (8) and (9) represents the integral value of the deterioration function dependency of x and f as written in (9) and (10):

$$F(b,f) = \frac{2}{b}\int_0^{b/2} \eta(x,f)\,\mathrm{d}x \tag{9}$$

$$\eta(x,f) = \begin{cases} 1 - \dfrac{x}{\delta} - a\dfrac{x}{\delta}\left(1 - \dfrac{x}{\delta}\right), & x < \delta \\ 0, & x \geq \delta \end{cases} \tag{10}$$

The continuous LMM allows a physical consideration of the material deterioration in FE simulation. This is possible with the influence depth δ, resulting from the model, and the magnetic permeability depending on the location and the magnetic field strength (Elfgen *et al.*, 2016a, 2016b).

3.2 Cut-edge length-dependent loss model

In the CLM, the cut lengths of the stator S_{Stat} and the rotor S_{Rot} are determined separately. To identify loss parameters used for the simulation, the equivalent cut-edge length of the stator S'_{Stat} and the rotor S'_{Rot} needs to be calculated using the following formula:

$$\begin{aligned} S'_{\mathrm{Stat}} &= S_{\mathrm{Stat}}\frac{w_{\mathrm{tot}}l_{\mathrm{tot}}}{A_{\mathrm{Stat}}} \\ S'_{\mathrm{Rot}} &= S_{\mathrm{Rot}}\frac{w_{\mathrm{tot}}l_{\mathrm{tot}}}{A_{\mathrm{Rot}}} \end{aligned} \tag{11}$$

where A_{Stat} is the area of the stator lamination and the rotor. First, the measured data (Figure 2) are linearly interpolated by the equivalent cut-edge length of the stator S'_{Stat} and the rotor S'_{Rot} to get equivalent losses. For the identification of the loss parameters, the methodology introduced in Elfgen *et al.* (2017) is used. All geometrical and loss parameters of the studied PMSM and the material M270-35A can be found in Table I.

Parameter		Stator	Rotor
Cut edge length	S	4,497.6 mm	3,880.2 mm
Equivalent cut edge length	S'	4,880.1 mm	6,834.4 mm
Area of lamination	A	13,271.4 mm^2	8,157.6 mm^2
Hysteresis loss parameter	a_1	0.0174	0.0205
Hysteresis loss exponent	α	2.06	1.87
Eddy current loss parameter	a_2	4.45×10^{-5}	4.45×10^{-5}
Saturation loss parameter	a_3	0.324	0.399
Saturation loss exponent	a_4	1.37	0.906
Excess loss parameter	a_5	6.54×10^{-4}	7.26×10^{-4}

Table I. Geometrical parameters of PMSM and loss parameters

3.3 Local iron loss model

For a physical representation, the material deterioration must be considered by the continuous and local material model as well as a LIM. It is well known that iron losses and iron loss parameters depend on mechanical stress introduced into the material (Karthaus *et al.*, 2017; Elfgen *et al.*, 2017). By combining the information of the general residual stress distribution from a mechanical or thermal cut (Maurel *et al.*, 2003; Siebert *et al.*, 2014; Schoppa *et al.*, 2000), the general behaviour of each iron loss parameters can be derived. The iron loss formulation in (1-5) receives a local dependence of both the flux density and the iron loss components as shown in (9). Each parameter of a_i (x) is described according to its behaviour of material degradation as shown in formula (12). First is the hysteresis, second the classical eddy currents, third the nonlinear iron losses and last the excess losses. A detailed explanation on the iron loss mechanism can be found in Steentjes *et al.* (2013):

$$P_{\mathrm{Fe}}(x,H,f) = a_1(x)B(x,f)^{\alpha(x)}f + a_2B(x,f)^2f^2 + a_2a_3(x)B(x,f)^{a_4(x)+2}f^2 + a_5(x)B(x,f)^{1.5}f^{1.5} \tag{12}$$

Thereby the iron loss calculation considers the nonlinear continuous LLM like the one introduced in (7) along with the frequency dependency of the material degradation. As the eddy current loss parameter a_2 is calculated analytically with

$$a_2 = \frac{\pi^2 d^2}{6\rho\rho_{\mathrm{e}}} \tag{13}$$

In terms of the material, it only depends on the electrical conductivity ρ_{e}, thickness d and mass density ρ. Those material-specific parameters are not affected by the stress. Hence, the eddy loss parameter is considered to be equal for all specimens. According to (9), the iron loss calculation does not depend on geometrical sizes such as the strip width but rather on the distance to the cut edge. To identify the model parameters, SST measurements of different strip width b_i are used. The integral value of the local iron loss formulation in (14) must describe the measured iron losses resulting from each specimen:

$$P_{\mathrm{Fe}}(b_i,B,f) = \frac{1}{b}\int_{-b_i/2}^{b_i/2} P(x,H,f)\mathrm{d}x \tag{14}$$

Owing to the elongated formulation to identify the iron loss components, the necessary equation system (15) is written only for hysteresis losses:

$$P_{\mathrm{hyst}}(b_i,B,f) = \frac{1}{b}\int_{-b_i/2}^{b_i/2} a_1(x)\left(\mu_0 H\left(\mu_{\mathrm{r,u}}(H,f) - \Delta\mu_{\mathrm{cut}}(H,f)\,\eta(x)\right)^{\alpha(x)}\right)\mathrm{d}x \tag{15}$$

The resulting local loss parameters normalized to the corresponding undamaged parameter $a_{\mathrm{i,und}}$ and the influence depth of the cut edge δ are depicted in Figure 3. The penetration depth perpendicular to the cutting edge is a model parameter of the continuous LLM and

depends on the used cutting technique and material (Elfgen *et al.*, 2016b) as shown in (10). A major share of the increase in iron losses is within the first millimetres of the degradation. As the local iron loss mechanism counteracts the local flux density distribution, increased local and overall losses can be measured. Especially, the excess and hysteresis losses show a high sensitivity towards the cutting influence.

3.4 Electric machine finite-element model

For this study as a numerical experiment, a permanent magnet synchronous motor (PMSM) for full electric drivetrains is chosen. The data sheet of the motor is shown in Table II.

For the calculation of the entire motor torque speed map, the methodology such as the one introduced in Ruf *et al.* (2016) is used. The maps for current heat losses and the four iron loss components for the rotor and the stator are calculated separately. With this approach, a detailed study of the influence of each component on the vehicle range is possible. The vehicle range can then be calculated based on various drive cycles such as the one shown in Ruf *et al.* (2016).

3.5 Driving cycle model

For the estimation of the influence of the cutting effect, as well as the simulation methodology on the vehicle range, a simplified longitudinal vehicle model is used. The needed power in the drive cycle $P_{\mathrm{Cycle}}(t)$ can be calculated by (16) as introduced in Miller (2010):

$$P_{\mathrm{Cycle}}(t) = \left(F_{\mathrm{Roll}}(t) + F_{\mathrm{Air}}(t) + F_{\mathrm{Slope}}(t) + F_{\mathrm{Acc}}(t)\right)v(t), \tag{16}$$

where $v(t)$ is the velocity of the vehicle. The driving resistance forces are calculated using formulas (17-20) (Miller, 2010):

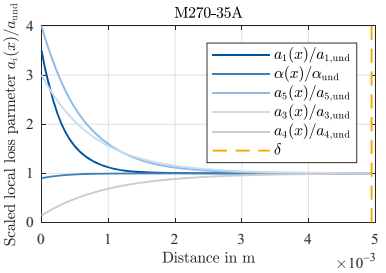

Figure 3.
Local loss parameters, scaled to the corresponding undamaged parameter and penetration depth δ

Specification		Value
Number of pole pairs	p	6
Stator inner diameter	d_{stat}	180 mm
Peak torque	T_{peak}	250 Nm
Peak power	P_{peak}	125 kW
Maximum electrical Fundamental frequency	$f_{\mathrm{el},max}$	1,200 Hz

Table II.
Technical data of the studied PMSM

$$F_{\text{Roll}} = f_{\text{fric}}\,(m_{\text{veh}} + m_{\text{add}})\cos(\varphi) \tag{17}$$

$$\mathrm{F}_{\text{Air}}(t) = \frac{1}{2}\,\rho_{\text{Air}}\,\mathrm{c_W}\,\mathrm{A}\,v(t)^2 \tag{18}$$

$$F_{\text{Slope}} = (m_{\text{veh}} + m_{\text{add}})\sin(\varphi) \tag{19}$$

$$F_{\text{Acc}} = (m_{\text{veh}} e_i + m_{\text{add}})\frac{\mathrm{d}v(t)}{\mathrm{d}t} \tag{20}$$

where F_{Roll} is the rolling friction, F_{Air} is the air friction, F_{Slope} is the slope and F_{Acc} is the acceleration force. A description of the vehicle model symbols, as well as the selected values representing a small city car, is shown in Table III.

The needed battery power of the electric car $P_{\text{Bat}}(t)$ is calculated based on the following formula:

$$P_{\text{Bat}}(t) = \eta_{\text{In,Bat}}^{\varepsilon}\,\eta_{\text{Mot}}(t)\,\eta_{\text{GB,Diff}}^{\varepsilon}\,P_{\text{Cycle}}(t) \tag{21}$$

The coefficient ε depends on the operation mode, i.e. $\varepsilon = 1$ for the driving mode and $\varepsilon = -1$ for the recuperation mode. To reduce model complexity, the combined efficiency of the inverter and the battery $\eta_{In,Bat}$ as well as the combined efficiency of the gearbox and the differential $\eta_{\text{GB,Diff}}$, are assumed to be constant with $\eta_{\text{In,Bat}} = 97$ per cent and $\eta_{\text{GB,Diff}} = 95$ per cent. In this study, additional influences are not considered in detail, as electric machine design parameters are in focus of the study. The efficiency of the electric motor $\eta_{\text{Mot}}(t)$ can be derived from the efficiency plots calculated in the electromagnetic finite element model (FEM). In this study, worldwide harmonized light vehicles test procedure class 3 of the worldwide harmonized light vehicles test procedure is used for the determination of the vehicle driving range. The length of the driving cycle is $r_{\text{Cycle}} = 23.3$ km, the duration is $t_{\text{Cycle}} = 1{,}800$ s and the usable battery energy is assumed to be $E_{\text{Bat}} = 25$ kWh. The range of the car is calculated on the basis of the following formulas:

$$P_{\text{Bat,avg}} = \frac{1}{t_{\text{Cycle}}}\int_{0\,\text{s}}^{t_{\text{Cycle}}} P_{\text{Bat}}(t)\,\mathrm{d}t \tag{22}$$

Table III.
Technical data of the vehicle model

Specification		Value
Friction coefficient	f_{fric}	0.01
Vehicle mass	m_{veh}	1,320 kg
Additional mass	m_{add}	425 kg
Slope angle	Φ	0°
Air density	ρ_{Air}	1.240 kg/m^3
Air friction coefficient	C_{W}	0.29
Vehicle cross section	A	2.38 m^2
Acceleration coefficient	e_i	1.2

$$r_{\mathrm{tot}} = r_{\mathrm{Cycle}} \frac{E_{\mathrm{Bat}}}{P_{\mathrm{Bat,avg}}\, t_{\mathrm{Cycle}}}, \tag{23}$$

where $P_{\mathrm{Bat,avg}}$ is the total average battery power used in the cycle.

4. Results

For the STM, a material model without considering the influence of cutting on the material permeability is used. The applied combinations of electric machine current densities in the direct J_{d} and quadrature J_{q} axes are shown in Figure 4. Depicted are the lines for constant output torque of the FEM, the maximum current line of 385 A and the maximum torque per ampere (MTPA) line of the control strategy in the base speed area. For the two models CLM and LIM, the same LLM in terms of the permeability is used (Elfgen *et al.*, 2016b). As the plotted torque does not include the losses in the machine, the lines for the two models are coincident. The local magnetic material degradation leads to an increased current demand of CLM and LIM in comparison with STM. The MTPA line is moved to higher currents with a more significant increase of the current in the quadrature axis.

The excess loss distribution as an example for one share of the iron losses referenced to the maximum occurring loss is shown in Figure 5. Therefore, the simulation with $J_{\mathrm{d}} = -2\ \mathrm{A/m^2}$ and $J_{\mathrm{q}} = 2\ \mathrm{A/m^2}$ is used. The distribution for CLM is shown in Figure 5(a) and that for LIM in Figure 5(b).

In the LIM, higher losses are calculated for the areas next to the cutting edge such as the stator teeth or the jokes of the rotor lamination. Because of the magnetic flux density concertation, losses increase in the centre of the geometry. In the case of the LIM, lower resulting iron losses in the centre result when compared with the CLM, as the loss parameters decrease strongly on the first few millimetres of the distance to the cut edge. Particularly at the stator teeth top local iron losses are underestimated by the CLM. An

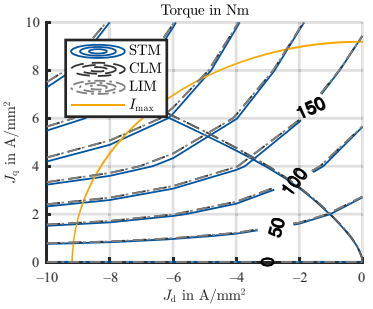

Figure 4.
Impact of material degradation on machine control strategy and torque

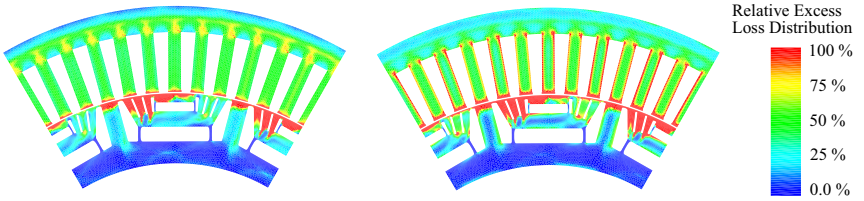

Figure 5.
Relative excess loss distribution for CLM and LIM for $J_{\mathrm{d}} = -2\ \mathrm{A/m^2}$ and $J_{\mathrm{q}} = 2\ \mathrm{A/m^2}$

overview of the losses in the entire driving cycle for the three studied models is shown in Table IV.

In the rotor, losses mainly occur in the area next to the outer radius of the lamination, i.e. in an area next to the cut edge (Figure 5). In the LIM, loss parameters representing a higher degradation are used in these local areas (Figure 3). This leads to higher rotor iron losses of the LIM in comparison with the CLM. This behaviour can be confirmed in the driving cycle calculations (Table IV). In the stator, the areas next to the cutting edge are magnetized with high frequencies and the entire lamination is magnetized with the electrical fundamental frequency. A significant share of losses occurs in areas away from the cutting edge such as the entire stator teeth or the entire stator yoke. In these areas, the global a priory model (CLM) uses loss parameters representing a higher degradation in comparison with the LIM that uses undamaged parameters (Figure 3). Thus, the resulting stator iron losses are less in the LIM than in the CLM (Table IV). The total iron losses for both simulation methodologies with considerations of cutting edges are comparable and increase in comparison with the STM without consideration of cutting edges. To keep the same output torque, the current needs to be increased, leading to higher copper losses, as shown in Table IV. Hence, total losses increase and the efficiency of the electric machine decreases. The comparison of the efficiency plots of the STM and the LIM is shown in Figure 6.

The consideration of the cutting effect leads to decreased efficiency, particularly in regions of the torque speed map with high rotational velocities, resulting in high electric frequencies and high iron losses in the electric motor lamination. The total loss in the driving cycle, as well as the driving range, is calculated based on formulas (15)–(23). The total losses of the simulations with consideration of the cutting effect (CLM and LIM) are comparable to each other and higher than the results of the model without cutting effect (STM). The vehicle range is reduced in the CLM by 2.4 per cent from 197.5 to 192.8 km and LIM by 2.3 per cent from 197.5 to 192.9 km in comparison to the STM.

Table IV.
Results of the vehicle range investigation

Result	STM	CLM	LIM
Iron loss rotor	147.3 W	183.8 W	204.9 W
Iron loss stator	378.9 W	492.2 W	467.7 W
Copper losses	120.6 W	124.1 W	124.1 W
Total loss	6,406.9 W	6,563.3 W	6,559.8 W
Vehicle range	197.5 km	192.8 km	192.9 km

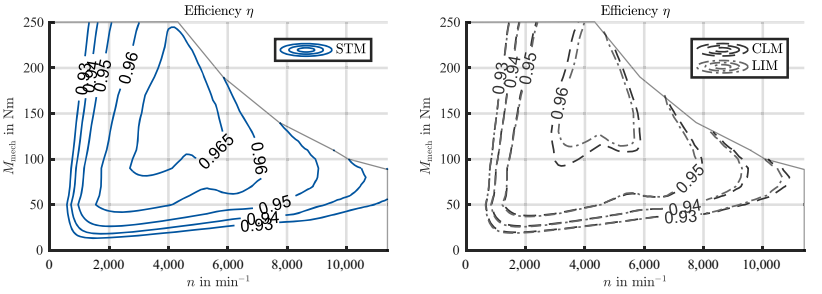

Figure 6.
Comparison of the efficiency plots of the STM, CLM and the LIM

6. Conclusions

Three different approaches for the calculation of iron losses have been presented and discussed. The model without consideration of cutting effect (STM) is used as the baseline for this study. In both models with consideration of the cutting effect (CLM and LIM), an LLM was described and used for the extraction of the field solution in the FEM. The methodology to calculate the global loss parameters used in the CLM was presented and discussed. The equivalent cut-edge length S' as a machine parameter can be seen as an impact factor of cutting edges on the increase of iron losses. Furthermore, the LIM was described and discussed. The impact of the material model and the loss calculation on a state-of-the-art PMSM was studied. Despite the reduced local flux density near the cut edge, a significant increase in local iron losses can be seen due to the cutting effect. Rotor iron losses are underestimated in the CLM in comparison with the LIM because the main share of losses for the rotor occurs in areas close to the cutting edge. In the stator, losses are overestimated in the CLM in comparison with the LIM, as a significant share of the losses occurs in areas away from the cutting edge such as the entire stator teeth and joke. The total losses for both models are comparable leading to the same decrease of the electric vehicle driving range. Thus, the cut-edge length iron loss model is a suitable methodology for the estimation of the impact of the cutting effect on overall efficiency. For a detailed investigation of the influences of the cutting effect in local areas, the usage of an LIM is indispensable.

References

Bali, M. and Muetze, A. (2017), "Influence of different cutting techniques on the magnetic characteristics of electrical steels determined by a permeameter", *IEEE Transactions on Industry Applications*, Vol. 53 No. 2, pp. 971-981.

Bertotti, G. (1988), "General properties of power losses in soft ferromagnetic materials", *IEEE Transactions on Magnetics*, Vol. 24 No. 1, pp. 621-630.

DIN German Institute for Standardization (2010), "Magnetic materials – part 3: methods of measurement of the magnetic properties of electrical steel strip and sheet by means of a single sheet tester (IEC 60404-3:1992 + A1:2002 + A2:2009)", No. DIN IEC 60404-3, Beuth Verlag, GmbH.

Eggers, D., Steentjes, S. and Hameyer, K. (2012), "Advanced iron-loss estimation for nonlinear material behavior", *IEEE Transactions on Magnetics*, Vol. 48 No. 11, pp. 3021-3024.

Elfgen, S., Ruf, A., Steentjes, S. and Hameyer, K. (2017), "Consideration of the manufacturing influence in standardized material characterizations using machine measurements", *2017 IEEE International Electric Machines and Drives Conference (IEMDC)*, *IEEE*, *Miami, FL*, 21.05.2017 – 24.05.2017, pp. 1-6.

Elfgen, S., Steentjes, S., Böhmer, S., Franck, D. and Hameyer, K. (2016a), "Continuous local material model for cut edge effects in soft magnetic materials", *IEEE Transactions on Magnetics*, Vol. 52 No. 5, pp. 1-4.

Elfgen, S., Steentjes, S., Böhmer, S., Franck, D. and Hameyer, K. (2016b), "Influences of material degradation due to laser cutting on the operating behaviour of PMSM using a continuous local material model", in *2016 XXII International Conference on Electrical Machines (ICEM), Lausanne, Switzerland, 04.09.2016 - 07.09.2016*, *IEEE*, pp. 1835-1840.

Karthaus, J., Elfgen, S. and Hameyer, K. (2017), "Behaviour of iron loss components dependent on mechanical compressive and tensile stress in Non-Oriented electrical steel", *18th International Symposium on Applied Electromagnetics and Mechanics (ISEM)*, Vincent Mazauri, Chamonix-Mont-Blanc.

Maurel, V., Ossart, F. and Billardon, R. (2003), "Residual stresses in punched laminations: Phenomenological analysis and influence on the magnetic behavior of electrical steels", *Journal of Applied Physics*, Vol. 93 No. 10, pp. 7106-7108.

Miller, J.M. (2010), *Propulsion Systems for Hybrid Vehicles, IET Renewable Energy Series*, 2nd ed., Institution of Engineering and Technology, Stevenage, Vol. 7.

Ruf, A., Steentjes, S., Pfingsten, G., von Grosse, T. and Hameyer, K. (Eds) (2016), *Requirements on Soft Magnetic Materials for Electric Traction Motors*, Centro Sviluppo Materiali S.P.A. (CSM), Rome.

Schoppa, A., Schneider, J. and Wuppermann, C.-D. (2000), "Influence of the manufacturing process on the magnetic properties of non-oriented electrical steels", *Journal of Magnetism and Magnetic Materials*, Vol. 215-216, pp. 74-78.

Siebert, R., Schneider, J. and Beyer, E. (2014), "Laser cutting and mechanical cutting of electrical steels and its effect on the magnetic properties", *IEEE Transactions on Magnetics*, Vol. 50 No. 4, pp. 1-4.

Siebert, R., Wetzig, A., Beyer, E., Betz, B., Grunzweig, C. and Lehmann, E. (2013), "Localized investigation of magnetic bulk property deterioration of electrical steel: analysing magnetic property drop thorough mechanical and laser cutting of electrical steel laminations using neutron grating interferometry", *2013 3rd International Electric Drives Production Conference (EDPC)*, Nuremberg, 29.10.2013 - 30.10.2013, *IEEE*, pp. 1-5.

Steentjes, S., Leßmann, M. and Hameyer, K. (2013), "Semi-physical parameter identification for an iron-loss formula allowing loss-separation", *Journal of Applied Physics*, Vol. 113 No. 17, p. 17A319.

Steentjes, S., Eggers, D., Leßmann, M. and Hameyer, K. (2012), "Iron-loss model for the FE-simulation of electrical machines", paper presented at 2012 Inductica Technical Conference, 26-28 June, Berlin.

Corresponding author
Benedikt Groschup can be contacted at: benedikt.groschup@iem.rwth-aachen.de